Conditional Physics-Informed Graph Neural Network for Fractional Flow Reserve Assessment

Baihong Xie[1], Xiujian Liu[1], Heye Zhang[1], Chenchu Xu[2,3], Tieyong Zeng[4], Yixuan Yuan[5], Guang Yang[6], and Zhifan Gao[1(✉)]

[1] School of Biomedical Engineering, Sun Yat-sen University, Shenzhen, China
gaozhifan@mail.sysu.edu.cn
[2] Institute of Artificial Intelligence, Hefei Comprehensive National Science Center, Hefei, China
[3] Anhui University, Hefei, China
[4] Department of Mathematics, The Chinese University of Hong Kong, Hong Kong, China
[5] Department of Electronic Engineering, The Chinese University of Hong Kong, Hong Kong, China
[6] Bioengineering Department and Imperial-X, Imperial College London, London, UK

Abstract. The assessment of fractional flow reserve (FFR) is significant for diagnosing coronary artery disease and determining the patients and lesions in need of revascularization. Deep learning has become a promising approach for the assessment of FFR, due to its high computation efficiency in contrast to computational fluid dynamics. However, it suffers from the lack of appropriate priors. The current study only considers adding priors into the loss function, which is insufficient to learn features having strong relationships with the boundary conditions. In this paper, we propose a conditional physics-informed graph neural network (CPGNN) for FFR assessment under the morphology and boundary condition information. Specially, CPGNN adds morphology and boundary conditions into inputs to learn the conditioned features and penalizes the residual of physical equations and the boundary condition in the loss function. Additionally, CPGNN consists of a multi-scale graph fusion module (MSGF) and a physics-informed loss. MSGF is to generate the features constrained by the coronary topology and better represent the different-range dependence. The physics-informed loss uses the finite difference method to calculate the residuals of physical equations. Our CPGNN is evaluated over 183 real-world coronary observed from 143 X-ray and 40 CT angiography. The FFR values of CPGNN correlate well with FFR measurements r = 0.89 in X-ray and r = 0.88 in CT.

Supplementary Information The online version contains supplementary material available at https://doi.org/10.1007/978-3-031-43990-2_11.

H. Greenspan et al. (Eds.): MICCAI 2023, LNCS 14226, pp. 110–120, 2023.
https://doi.org/10.1007/978-3-031-43990-2_11

Keywords: Fractional Flow Reserve Assessment · Physics-Informed Neural Networks · Coronary Angiography

1 Introduction

The assessment of fractional flow reserve (FFR) is significant for diagnosing coronary artery disease (CAD) and determining the patients and lesions in need of revascularization [1,2]. Although CAD is widely diagnosed by angiography technique in routine, the anatomical markers often underestimate or overestimate a lesion's functional severity [3]. FFR is the gold standard for the functional diagnosis of CAD and guides the revascularization strategy, due to its ability to assess the ischemic potential of a stenosis [4]. According to a multicenter trial, the use of FFR recalls an additional 30% of severe stenosis required revascularization [5]. Additionally, another trial demonstrates a 5.1% reduction of the 1-year adverse event rate by using FFR [3]. Therefore, it advocates the routine use of FFR in the clinical practice guidelines of the European Society and American Heart Association [1,6]. However, the widespread adoption of FFR is restricted by the risk associated with maneuvering a pressure wire down a coronary artery and the added time to assess multiple vessels [7]. Therefore, it is an eager need for assessing FFR derived from angiography.

Deep learning has become a promising approach for the assessment of FFR, due to its high computation efficiency in contrast to the computational fluid dynamics [8–11]. However, it suffers from the lack of appropriate priors. An appropriate prior is challenging to be found, due to FFR being ruled by the complex physical process (i.e. Navier-Stokes equations) [12].

Physics-informed neural networks (PINNs) have the potential to address the aforementioned challenge of lacking appropriate priors. PINNs add priors to the loss function by penalizing the residual of physical equations and the boundary conditions [13]. This prior guides the learning to a direction in compliance with the physical principles and boundary conditions. For example, PINNs add the Navier-Stokes equations and the boundary conditions to the loss function to generate a physically consistent prediction of blood pressure and velocity on the arterial networks [14–16]. However, only adding the prior to the loss function is insufficient, because the learned features are weakly related to boundary conditions in the loss function.

In this paper, we apply a prior to the inputs. Adding boundary conditions as prior to the inputs resulting in a strong relationship between learned features and boundary conditions. Therefore, the learned features contain more direct and powerful boundary condition information. Additionally, a graph network is introduced as a prior to enforce the coronary topology constraint, because the interaction between the nodes on the graph is similar to the interaction of FFR between the spatial points on the coronary. To this end, we propose a conditional physics-informed graph neural network (CPGNN) for FFR assessment under the constraint of the morphology and boundary conditions. CPGNN adds morphology and boundary conditions as priors to the inputs for learning the conditioned

features, besides adding priors to the loss function by penalizing the residual of physical equations and the boundary conditions. Specially, CPGNN consists of a multi-scale graph fusion module (MSGF) and a physics-informed loss. The purpose of MSGF is to generate the features constrained by the coronary topology and better represents the different-range dependence. The physics-informed loss uses the finite difference method to calculate the residuals of physical equations.

The main contributions in the paper are three-fold:

(1) CPGNN provides FFR assessment under the condition of morphology and boundary.
(2) CPGNN introduces a prior by adding the information of the morphology and boundary into inputs and a multi-scale graph fusion module is designed to capture the conditional features related to those information.
(3) The extensive experiments on the 6600 synthetic coronary and 183 clinical angiography including 40 CT and 143 X-ray. The performance of our CPGNN demonstrates the advantages over six existing methods.

2 Method

2.1 Problem Statement

The purpose of CPGNN is to add the appropriate prior, which makes sure that the prediction of blood pressure and flow meet boundary conditions and the conservation of physical principle. The idea is to find a loss term describing the rules of blood pressure and flow. There exists the hemodynamic theory [12] to solve the pressure Q and flow P on spatial coordinate z, which is defined as:

$$\begin{cases} \mathcal{F}(Q(z), P(z); \theta) = 0 & z \in \Omega \\ \mathcal{B}(Q(z), P(z); \gamma) = 0 & z \in \partial\Omega \end{cases} \tag{1}$$

where Ω is the domain of the coronary, $\partial\Omega$ is the boundary, θ is the morphology parameters, γ is boundary condition, $\mathcal{F}$ and $\mathcal{B}$ are operators to describe the control equation and boundary constraints respectively.

A neural network with parameter ω is introduced to approximate the pressure and flow, defined as $Q_\omega(z)$ and $P_\omega(z)$. Then, the residuals of the Eq. (1) can be added to the loss function as prior. The prediction can be constrained by minimizing the residuals on coronary, namely

$$\arg\min_{\omega} \int_{\Omega} \|\mathcal{F}(Q_\omega(z), P_\omega(z); \theta)\|_2 \, dz + \int_{\partial\Omega} \|\mathcal{B}(Q_\omega(z), P_\omega(z); \gamma)\|_2 \, dz \tag{2}$$

Further, considering the feature learned by Eq. (2) have a weak relation with the γ and θ, both are added as prior conditional inputs to approximate the flow $Q_\omega(z|\gamma, \theta)$ and pressure $P_\omega(z|\gamma, \theta)$ by the process:

$$\begin{aligned} \arg\min_{\omega} \int_{\Omega} \|\mathcal{F}(Q_\omega(z|\gamma, \theta), P_\omega(z|\gamma, \theta))\|_2 \, dz \\ + \int_{\partial\Omega} \|\mathcal{B}(Q_\omega(z|\gamma, \theta), P_\omega(z|\gamma, \theta))\|_2 \, dz \end{aligned} \tag{3}$$

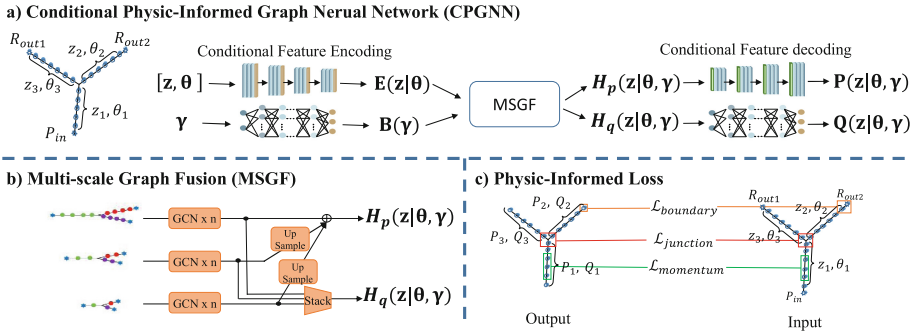

Fig. 1. The architecture of CPGNN. The morphology θ and boundary γ are added into the inputs. The multi-scale graph fusion is used to enforce the constraint from coronary topology and capture the different-range dependency. The physics-informed loss is used to guide conditional features encoding

2.2 Conditional Physics-Informed Graph Neural Network

As shown in the Fig. 1, CPGNN contains an encoding-decoding architecture to predict the pressure and flow, by the produce:

$$Q(z|\theta,\gamma), P(z|\theta,\gamma) = decoder(MSGF(embedding(\gamma), encoder(z,\theta))) \quad (4)$$

According to hemodynamic theory [12], the morphology θ is the cross-sectional area, and boundary condition γ consists of the outlet resistances and inlet pressure. By sampling uniformly on coronary, the inputs of CPGNN the morphology $\theta \in R^{N_v \times N_d \times 1}$, the spatial coordinate $Z \in R^{N_v \times N_d \times 1}$ and the boundary condition $\gamma \in R^{N_b \times 1}$. The N_v, N_d, and N_b are the number of vessel branches, sampling points, and coronary boundary.

Conditional Feature Encoding. The θ is directly combined with Z, due to their corresponding relation. A serial of 1D convolution and down-sampling is used to generate the morphology features $M(z|\theta) \in R^{N_v \times N_d/8 \times C}$. There is a full connection layer to embed the vector γ into $B(\gamma) \in R^{N_b \times C}$.

Multi-scale Graph Fusion. The graph convolution operator is introduced to enforce the coronary topology constraint. The morphology features $M(z|\theta)$ compose the graph on coronary. The graph adds $B(\gamma)$ as new points at the corresponding boundary. Besides, a multi-scale mechanism is introduced to enhance the representation of the features, because it is beneficial to capture the different-range dependency. According to the hemodynamic theory [12], the flow is constant on the branch due to mass conservation under steady-state one-dimensional modeling, and the pressure varies associated with the position. The feature $H_p(z|\theta,\gamma) \in R^{N_v \times N_d/8 \times C}$ is obtained by the element-wise fusion on up-sampling

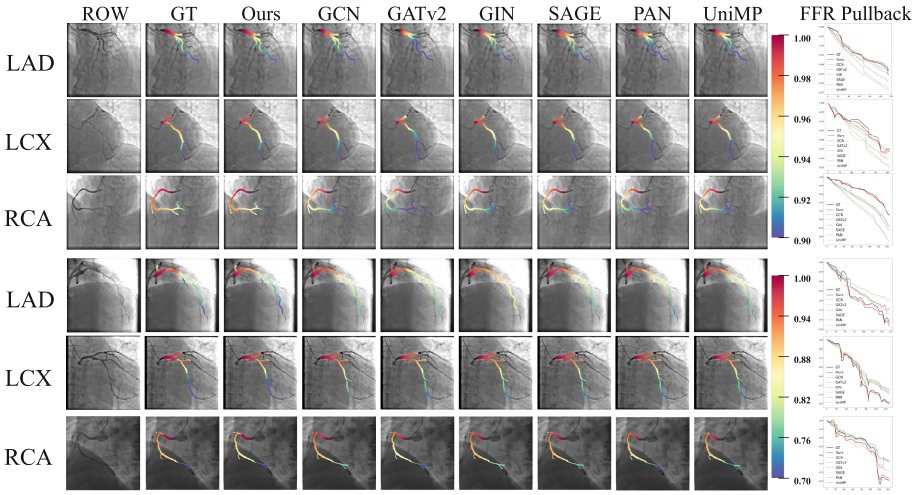

Fig. 2. Representative pressure predictions show our CPGNN is better than other state-of-the-art methods on the X-ray angiography data

feature graphs while the feature $H_q(z|\theta,\gamma) \in R^{N_v \times N_q \times C}$ is obtained by concatenating feature graphs at the branch channel. The N_q is the concatenated dimension according to the number of feature graphs used to fuse.

Conditional Feature Decoding. A serial of 1D convolution and up-sampling is used to decode the feature $H_p(z|\theta,\gamma)$ and generate the pressure prediction $P(z|\theta,\gamma) \in R^{N_v \times N_d \times 1}$. Considering the conversation of the mass, the points share the same prediction on branch. Thus, a full connection layer is used to decode the feature $H_q(z|\theta,\gamma)$ to generate the flow prediction $Q(z|\theta,\gamma) \in R^{N_v \times 1}$

Momentum Loss. The pointset $D = (Z, S, Q, P)$ contain the coordinate Z, cross-sectional area S, flow Q, and pressure P of the points at the coronary. The vessel wall is assumed to be rigid and blood is Newtonian fluid. The momentum loss term combines the hemodynamic equation and finite differences [12,17], defined as

$$\mathcal{L}_m = \frac{1}{N_v}\frac{1}{N_d}\sum_{i=1}^{N_v}\sum_{j=1}^{N_d}\left(\sum_{k=k_{min}}^{k_{max}}\frac{N_k}{Dh_i}\left(\frac{4}{3}\frac{Q_{i,j+k}^2}{S_{i,j+k}}+\frac{S_{i,j}P_{i,j+k}}{\rho}\right)+C\frac{Q_{i,j}}{S_{i,j}}\right)^2 \quad (5)$$

where (i, j) denote the j-th point at the i-th branch , N_d is point number on branch, N_v is branch number on coronary, h_i is the point interval on i-th branch defined as $h_i = (Z_{i,N_d} - Z_{i,1})/(N_d - 1)$, C is a coefficient describing the stenosis influence defined in [12].

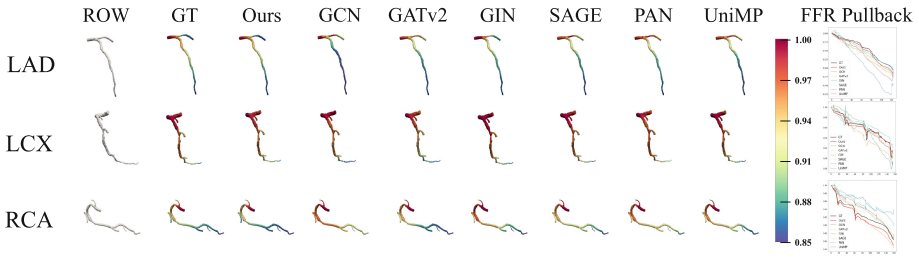

Fig. 3. Representative pressure predictions show our CPGNN is better than the other six state-of-the-art methods on the CT data.

Junction Loss. Given the pointset $J = (Q, P)$ containing flow Q and pressure P of the points at the branch junction, the conservation of momentum and mass is constrained by

$$\mathcal{L}_j = \frac{1}{N_j}\sum_{i=1}^{N_j}\left(\sum_{j=1}^{N_p^i} Q_{i,j}\right)^2 + \sum_{j=2}^{N_p^i}\left(P_{i,1} + \frac{\rho}{2}\left(\frac{Q_{i,1}}{S_{i,1}}\right)^2 - P_{i,j} - \frac{\rho}{2}\left(\frac{Q_{i,j}}{S_{i,j}}\right)^2\right)^2 \quad (6)$$

where N_j is the number of junction on coronary tree, N_p^i is the number of points of the i-th junction, (i, j) denotes the j-th point at the i-th junction and the 1-st point is the nearest point to the coronary inlet.

Boundary Loss. Given the pointset $B = (Q, P, \gamma)$ containing flow Q, pressure P and condition γ of the points at the boundary, the boundary constraint is penalized by

$$\mathcal{L}_b = (P_1 - \gamma_1)^2 + \frac{1}{N_b}\sum_{i=2}^{N_b}(P_i - Q_i\gamma_i)^2 \quad (7)$$

where N_b is the number of boundary, the 1-st point is inlet, the rest points are outlet. Eventually, the objective of our CPGNN is to minimize the total loss $\mathcal{L}_{total}$:

$$\mathcal{L}_{total} = \mathcal{L}_m + \lambda_1\mathcal{L}_j + \lambda_2\mathcal{L}_b \quad (8)$$

where λ_1 and λ_2 are the trade-off parameters.

3 Experiments and Results

3.1 Materials and Experiment Setup

The experiment contains one synthetic dataset and two in-vivo datasets. (1) the synthetic data. We generate 6600 synthetic coronary trees for training. The parameters of geometry and boundary conditions are randomly set in the appropriate ranges, including vessel radius, the length and number of branches, inlet

Table 1. Comparison of our CPGNN and six state-of-the-arts methods for pressure prediction on synthetic data. LAD, left anterior descending artery; LCX, left circumflex artery; RCA, right coronary artery.

method	ALL			LAD			LCX			RCA		
	MAE	RMSE	MAPE	MAE	RMSE	MAPE	MAE	RMSE	MAPE	MAE	RMSE	MAPE
GCN [22]	1.17	1.32	1.25	0.94	1.08	1.00	0.91	1.08	0.97	1.65	1.77	1.77
GATv2 [23]	2.22	2.57	2.40	1.77	2.11	1.90	1.71	2.08	1.84	3.18	3.51	3.45
GIN [24]	1.22	1.35	1.31	1.04	1.16	1.11	1.01	1.15	1.07	1.62	1.72	1.73
SAGE [25]	1.15	1.29	1.22	0.92	1.06	0.98	0.91	1.08	0.97	1.60	1.73	1.72
PAN [26]	2.03	2.34	2.19	1.62	1.91	1.74	1.56	1.90	1.68	2.90	3.19	3.15
UniMP [27]	1.48	1.65	1.59	1.26	1.42	1.35	1.23	1.43	1.32	1.96	2.10	2.11
Our CPGNN	**0.74**	**0.86**	**0.79**	**0.67**	**0.79**	**0.71**	**0.65**	**0.76**	**0.69**	**0.90**	**1.01**	**0.96**

Table 2. Ablation of the number of graph scale levels and the conditional inputs on both synthetic data and in-vivo data. The S1, S2, and S3 represent the number of graphs are 1, 2, and 3

conditional inputs		graph number			synthetic data					X-ray	CT
θ	γ	S1	S2	S3	MAE	RMSE	MAPE	$\mathcal{L}_{mom}$	$\mathcal{L}_{junc}$	AUC	AUC
		✓			45.71	55.82	52	7.34	21.44	0.568	0.538
	✓	✓			41.45	50.38	45	7.14	17.36	0.63	0.549
✓		✓			19.89	23.95	21	6.20	9.44	0.742	0.632
✓	✓	✓			1.15	1.32	1.21	5.09	1.39	0.917	0.786
✓	✓		✓		1.06	1.18	1.11	3.15	1.60	0.93	0.84
✓	✓			✓	**0.74**	**0.86**	**0.79**	**2.59**	**1.17**	**0.97**	**0.93**

pressure, and outlet resistances [18]. The pressure ground truth (GT) is simulated by Simvascular [12]. (2) the in-vivo data. There are 143 X-ray and 40 CT angiography from 183 patients. The acquisition process obeys the standard clinical practice [19]. The setting of the boundary conditions is based on the TIMI count method [20] and PP-outlet strategy [21]. The FFR was performed using pressure guide-wire by the manufacturer Abbott with model HI-TORQUE for all patients in the clinic dataset.

All experiments run on a platform with NVIDIA RTX A6000 48 GB GPU. The Adam optimizer is used with 16 batch size per step. Initial learning rate is 0.001 and the decay rate is 0.95. The ratio of the training and verification of the synthetic dataset is 8:2. CPGNN is trained on the synthetic dataset and tested on both synthetic and clinical datasets.

CPGNN is compared with six state-of-the-art methods, GCN [22], GATv2 [23], GIN [24], SAGE [25], PAN [26] and UniMP [27]. The evaluation metrics are Root Mean Square Errors (RMSE), Mean Absolute Errors (MAE), Mean Absolute Percentage Errors (MAPE), the residual of momentum equation ($\mathcal{L}_{mom}$) and the residual of junction equation ($\mathcal{L}_{junc}$). The units of RMSE, MAE, $\mathcal{L}_{mom}$ and $\mathcal{L}_{junc}$ are mmHg, mmHg, e^{-6} and e^{-2}.

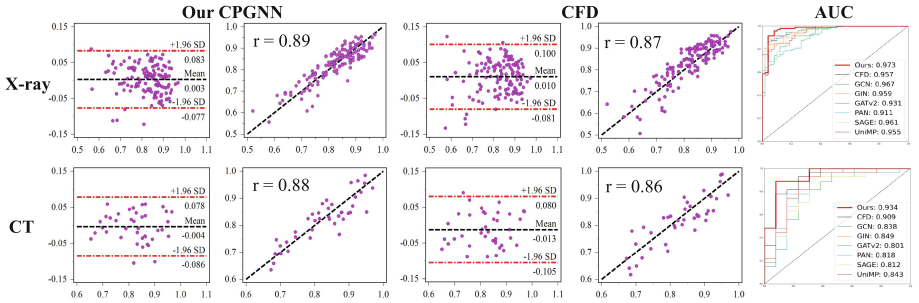

Fig. 4. Comparison of our CPGNN with computational fluid dynamics (CFD) for FFR assessment. The ground truth is in-vivo FFR measurement. The Bland-Altman analysis and Pearson correlation are performed for both CPGNN and CFD. The area under the curve (AUC) of CPGNN, CFD, and six state-of-the-art methods for the stenosis diagnosis (FFR<0.8) is performed

3.2 Results on Synthetic Data

Comparison of Pressure Prediction: The performance of CPGNN is closer to the GT with an overall MAE of 0.74, RMSE of 0.86, and MAPE of 0.79. Table 1 shows that CPGNN performs well than six state-of-the-art methods.

Ablation of Conditional Inputs and Multi-scale Mechanism: As shown in Table 2, the prediction of PINNs has a poor performance on unseen coronary without the morphology and boundary condition inputs. Thus, it is necessary to add both as inputs. The results gradually improve MAE, RMSE, and MAPE from 1.15 to 0.74, 1.32 to 0.86, and 1.21 to 0.79 when adding the number of graph scale-level. Thus, the multi-scale mechanism plays a key role.

3.3 Results on In-Vivo Data

Comparison of FFR Assessment: As shown in Fig. 4, Bland-Altman analysis and Pearson correlation are conducted to evaluate the differences between CPGNN and in-vivo FFR measurement based on X-ray and CT data. Compared to the computational fluid dynamics, CPGNN has a well consistency with in-vivo FFR in the Fig. 4. Figure 2 and Fig. 3 directly display FFR results of CPGNN and six state-of-the-art methods. Figure 4 presents the area under curve (AUC) of CPGNN is best for the stenosis diagnosis (FFR<0.8). Those results demonstrate that CPGNN outperforms the other six existing methods in the clinical FFR assessment.

Ablation of CPGNN Components: As shown in Table 2, the AUC of different settings is shown. The results also demonstrate that the conditional inputs and the multi-scale mechanism are important for FFR Assessment in the clinic.

4 Conclusion

In this paper, we propose a conditional physics-informed graph neural network (CPGNN) for FFR assessment under the condition of morphology and boundary. Compared to the current reduce-order computation method [12], CPGNN does not need to couple stenosis detection algorithm and enable automatic stenosis feature extraction, which avoids error accumulation and achieves better performance. CPGNN introduces a prior by adding the information of the morphology and boundary into inputs and a multi-scale graph fusion module is designed to capture the conditional features related to those information. The method is conducted on 143 X-ray and 40 CT subjects. The performance of CPGNN is higher than the six state-of-the-art methods. The FFR of CPGNN correlates well with FFR measurements ($r = 0.89$ in X-ray and $r = 0.88$ in CT). The computation speed of CPGNN is 0.03 s per case, which is 600× faster than the SimVascular computation method [12]. Those results demonstrate that our CPGNN can aid in the clinical FFR assessment.

Acknowledgement. This work was supported in part by National Natural Science Foundation of China (62101606, 62276282, 62101610, 62106001, U1908211), Guangdong Basic and Applied Basic Research Foundation (2022A1515011384), the University Synergy Innovation Program of Anhui Province (GXXT-2021-007), and the Anhui Provincial Natural Science Foundation (2208085Y19).

References

1. Knuuti, J., Revenco, V., Saraste, A., et al.: 2019 ESC guidelines for the diagnosis and management of chronic coronary syndromes. Eur. Heart J. **41**(5), 407–477 (2020)
2. Neumann, F.-J., Sousa-Uva, M., Ahlsson, A., et al.: 2018 ESC/EACTS guidelines on myocardial revascularization. Eur. Heart J. **40**(2), 87–165 (2019)
3. Tonino, P.A.L., De Bruyne, B., Pijls, N.H.J., et al.: Fractional flow reserve versus angiography for guiding percutaneous coronary intervention. New England J. Med. **360**(3), 213–224 (2009)
4. Pijls, N.H., Van Son, J.A., Kirkeeide, R.L., et al.: Experimental basis of determining maximum coronary, myocardial, and collateral blood flow by pressure measurements for assessing functional stenosis severity before and after percutaneous transluminal coronary angioplasty. Circulation **87**(4), 1354–1367 (1993)
5. Tonino, P.A.L., Fearon, W.F., De Bruyne, B., et al.: Angiographic versus functional severity of coronary artery stenoses in the fame study: fractional flow reserve versus angiography in multivessel evaluation. J. Am. College Cardiol. **55**(25), 2816–2821 (2010)
6. Levine, G.N., Bates, E.R., Bittl, J.A., et al.: 2016 ACC/AHA guideline focused update on duration of dual antiplatelet therapy in patients with coronary artery disease: a report of the American college of cardiology/American heart association task force on clinical practice guidelines. Circulation **134**(10), e123–e155 (2016)
7. Tebaldi, M., Biscaglia, S., Fineschi, M., et al.: Evolving routine standards in invasive hemodynamic assessment of coronary stenosis: the nationwide Italian SICI-GISE cross-sectional ERIS study. JACC Cardiovasc. Interv. **11**(15), 1482–1491 (2018)

8. Li, Y., Qiu, H., Hou, Z., et al.: Additional value of deep learning computed tomographic angiography-based fractional flow reserve in detecting coronary stenosis and predicting outcomes. Acta Radiol. **63**(1), 133–140 (2022)
9. Gao, Z., Wang, X., Sun, S., et al.: Learning physical properties in complex visual scenes: an intelligent machine for perceiving blood flow dynamics from static CT angiography imaging. Neural Netw. **123**, 82–93 (2020)
10. Itu, L., Rapaka, S., Passerini, T., et al.: A machine-learning approach for computation of fractional flow reserve from coronary computed tomography. J. Appl. Physiol. **121**(1), 42–52 (2016)
11. Zhang, D., Liu, X., Xia, J., et al.: A physics-guided deep learning approach for functional assessment of cardiovascular disease in IoT-based smart health. IEEE Internet Things J. (2023)
12. Updegrove, A., Wilson, N.M., Merkow, J., et al.: SimVascular: an open source pipeline for cardiovascular simulation. Ann. Biomed. Eng. **45**, 525–541 (2017)
13. Raissi, M., Perdikaris, P., Karniadakis, G.E.: Physics-informed neural networks: a deep learning framework for solving forward and inverse problems involving nonlinear partial differential equations. J. Comput. Phys. **378**, 686–707 (2019)
14. Fathi, M.F., Perez-Raya, I., Baghaie, A., et al.: Super-resolution and denoising of 4D-flow MRI using physics-informed deep neural nets. Comput. Methods Programs Biomed. **197**, 105729 (2020)
15. Sarabian, M., Babaee, H., Laksari, K.: Physics-informed neural networks for brain hemodynamic predictions using medical imaging. IEEE Trans. Med. Imaging **41**(9), 2285–2303 (2022)
16. Kissas, G., Yang, Y., Hwuang, E., et al.: Machine learning in cardiovascular flows modeling: predicting arterial blood pressure from non-invasive 4D flow MRI data using physics-informed neural networks. Comput. Methods Appl. Mech. Eng. **358**, 112623 (2020)
17. Eberly, D.: Derivative Approximation by Finite Differences. Magic Software Inc. (2008)
18. El Sayed, S., El Sawa, E.A., Atta-Alla, A.E.S., et al.: Morphometric study of the right coronary artery. Int. J. Anat. Res. **3**(3), 1362–1370 (2015)
19. Di Mario, C., Sutaria, N.: Coronary angiography in the angioplasty era: projections with a meaning. Heart **91**(7), 968–976 (2005)
20. Tu, S., Barbato, E., Köszegi, Z., et al.: Fractional flow reserve calculation from 3-dimensional quantitative coronary angiography and TIMI frame count: a fast computer model to quantify the functional significance of moderately obstructed coronary arteries. JACC Cardiovasc. Interv. **7**(7), 768–777 (2014)
21. Liu, X., Chuangye, X., Rao, S., et al.: Physiologically personalized coronary blood flow model to improve the estimation of noninvasive fractional flow reserve. Med. Phys. **49**(1), 583–597 (2022)
22. Kipf, T.N., Welling, M.: Semi-supervised classification with graph convolutional networks. In: International Conference on Learning Representations (2017)
23. Brody, S., Alon, U., Yahav, E.: How attentive are graph attention networks? In: International Conference on Learning Representations (2022)
24. Xu, K., Hu, W., Leskovec, J., et al.: How powerful are graph neural networks? In: International Conference on Learning Representations (2019)
25. Hamilton, W.L., Ying, R., Leskovec, J.: Inductive representation learning on large graphs. In: International Conference on Neural Information Processing Systems (2017)

26. Ma, Z., Xuan, J., Wang, Y.G., et al.: Path integral based convolution and pooling for graph neural networks. In: International Conference on Neural Information Processing Systems (2020)
27. Shi, Y., Huang, Z., Feng, S., et al.: Masked label prediction: unified message passing model for semi-supervised classification. In: International Joint Conference on Artificial Intelligence (2021)